

Zhengpu LIN

OCE326 Ocean Engineering Design IV: Resource Exploitation and Equipment Course report summary

2023 Autumn



*This report is dedicated
to OCE326 for the fall
2023 semester, a nice
experience.*

Contents

1 Seawater desalination process design	3
1.1 Background	3
1.2 Reverse osmosis process	3
1.3 Plan I	3
1.4 Plan II	3
2 Finite element simulation of chloride ion infiltration based on comsol	5
2.1 Backgound	5
2.2 Requirement of project	5
2.3 Simulated Result	8
2.4 Appendix	8
3 Finite element simulation of offshore wind turbine based on fluid-structure coupling	10
3.1 Background	10
3.2 Simulation preparation	10
3.3 Simulated Result	11
3.4 Difficulties encountered in the simulation	11
4 Finite element simulation and failure study of lateral well	13
4.1 Background	13
4.2 Simulation preparation	13
4.2.1 Fluid flow	14
4.2.2 Solid Deformation	14
4.2.3 Failure Criterion	14
4.3 Simulated Result	14
5 Acknowledgments	20



1 SEAWATER DESALINATION PROCESS DESIGN

1.1 BACKGROUND

Osmosis is a physical phenomenon by which two liquids, in different concentrations, separated by a semi-permeable membrane, come into contact and tend to even themselves out. The liquid with the lower concentration crosses the membrane toward that with the highest concentration.

This process is inverted in reverse osmosis. We take in seawater, a highly concentrated solution, and force it through the membrane by adding pressure. On the other side, we obtain salt-free water, while back on the first side the remaining water still holds the salt the membrane prevented from passing through.

1.2 REVERSE OSMOSIS PROCESS

In reverse osmosis desalination, water is taken from the sea and receives a first treatment to eliminate impurities, oil, seaweed, rubbish, and so on. Once free of organic substances, the saltwater can be subjected to reverse osmosis. After the filtering, we have two streams: one brine and the other freshwater. The brine solution is diluted before being returned to the sea, avoiding high concentrations of salt which could harm the ecosystem. The freshwater passes through a remineralization and chlorination process, after which it is stored in tanks and then sent to the distribution network for consumption.

Reverse osmosis is not only the most advanced desalination system in the world today, but it is also the most efficient and beneficial for the planet: it generates up to four-and-a-half-times fewer greenhouse gas emissions than all other technologies, it doesn't harm the marine environment, and it's able to recover a large part of the energy used in the process.

1.3 PLAN I

One pass and two stages, because the recovery rate is 50%, the water production flow rate is $40000m^3/d$, and the inflow flow rate is $80000m^3/d$, SW30HRLE-440 membrane is selected, the number of cores is 6. Through calculation, the number of components required is 2670, 297, and 148 in the first and second stages respectively.

$$\text{Total membrane elements} = \frac{\frac{40000m^3/d}{5.451m^3/d} \times 1440\text{grd}}{9gfd \times 440ft^2} = 2670, \frac{2670}{6} = 445$$

1.4 PLAN II

Two pass and two stages, because the recovery rate is 50%, the water production flow rate is $40000m^3/d$, the inflow flow rate is $80000m^3/d$, SW30HRLE-440 membrane is selected, the number of cores is 6, and the recovery rate of the second pass is 80%. Through calculation, the water production of the second pass is $40000m^3/d$. The total number of components required for the second pass is



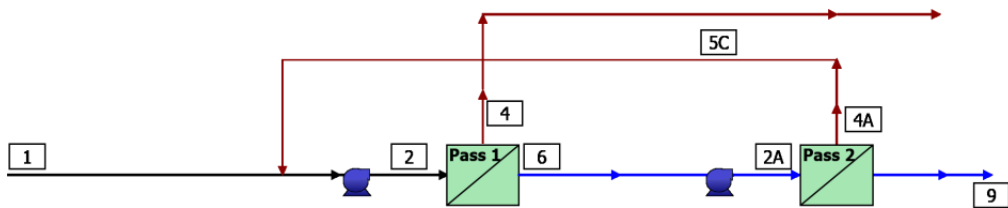


FIGURE 1: PLAN I: ONE PASS AND TWO STAGES

2670, the first stage is 297 and the second stage is 148 (generally a 2:1 ratio); The water yield of the first pass is $5000m^3$ and the total number of components required for the first pass is 3336, 371 and 185 respectively for the first stage and the second stage. The concentrated water after the second pass of filtration is returned to the first pass before the re-penetration.

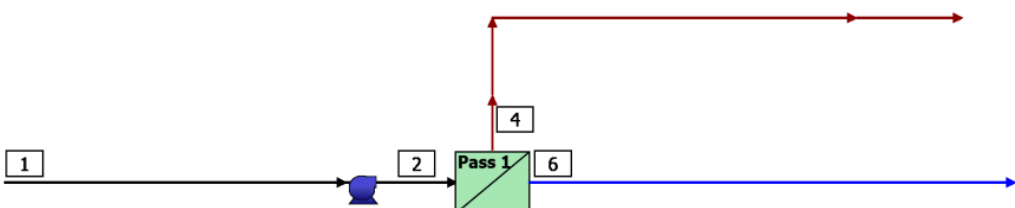


FIGURE 2: PLAN II: TWO PASS AND TWO STAGES

$$\text{The second stage membrane elements} = \frac{\frac{40000m^3/d}{5.451m^3/d} \times 1440grd}{9gfd \times 440ft^2} = 2670, \frac{2670}{6} = 445$$

$$\text{The first stage membrane elements} = \frac{\frac{50000m^3/d}{5.451m^3/d} \times 1440grd}{9gfd \times 440ft^2} = 3336, \frac{3336}{6} = 556$$

For plan II, there are two different groups of choices, respectively adding NaOH before the second stage and not adding NaOH. The final pH is 8.4 and 6.4, and other parameters are roughly the same.

Compared with the two schemes, the energy consumption of the former is $4.27kWh/m^3$, the energy consumption of the latter is $5.14kWh/m^3$, and the energy consumption of the first plan is less.

2 FINITE ELEMENT SIMULATION OF CHLORIDE ION INFILTRATION BASED ON COMSOL

2.1 BACKGROUND

Marine atmospheric exposure conditions provide a severe environment for reinforced concrete structures, mainly due to the occurrence of chloride-induced reinforcement corrosion. Chloride-induced corrosion of reinforcing steel is the main issue affecting the durability of reinforced concrete (RC) structures in coastal environments. Corrosion of rebars usually requires repair or replacement of RC elements, resulting in huge maintenance costs, out-of-service time, and waste of materials and energy. The maintenance cost of concrete bridges in developed countries, such as the United States, Canada, Japan, Australia, and the United Kingdom, has accounted for 0.01% to 0.1% of the gross domestic product in recent years. Growing attention has been paid to accurate predictions of chloride penetration in concrete worldwide.

The penetration of chloride ions in concrete is a complicated process, and diffusion is generally regarded as the primary transport mechanism in present service life calculations. Collepardi was the first who studied the diffusion characteristics of chloride ions in concrete based on Fick's second law.

$$\frac{\partial C}{\partial t} = D \frac{\partial^2 C}{\partial x^2}$$

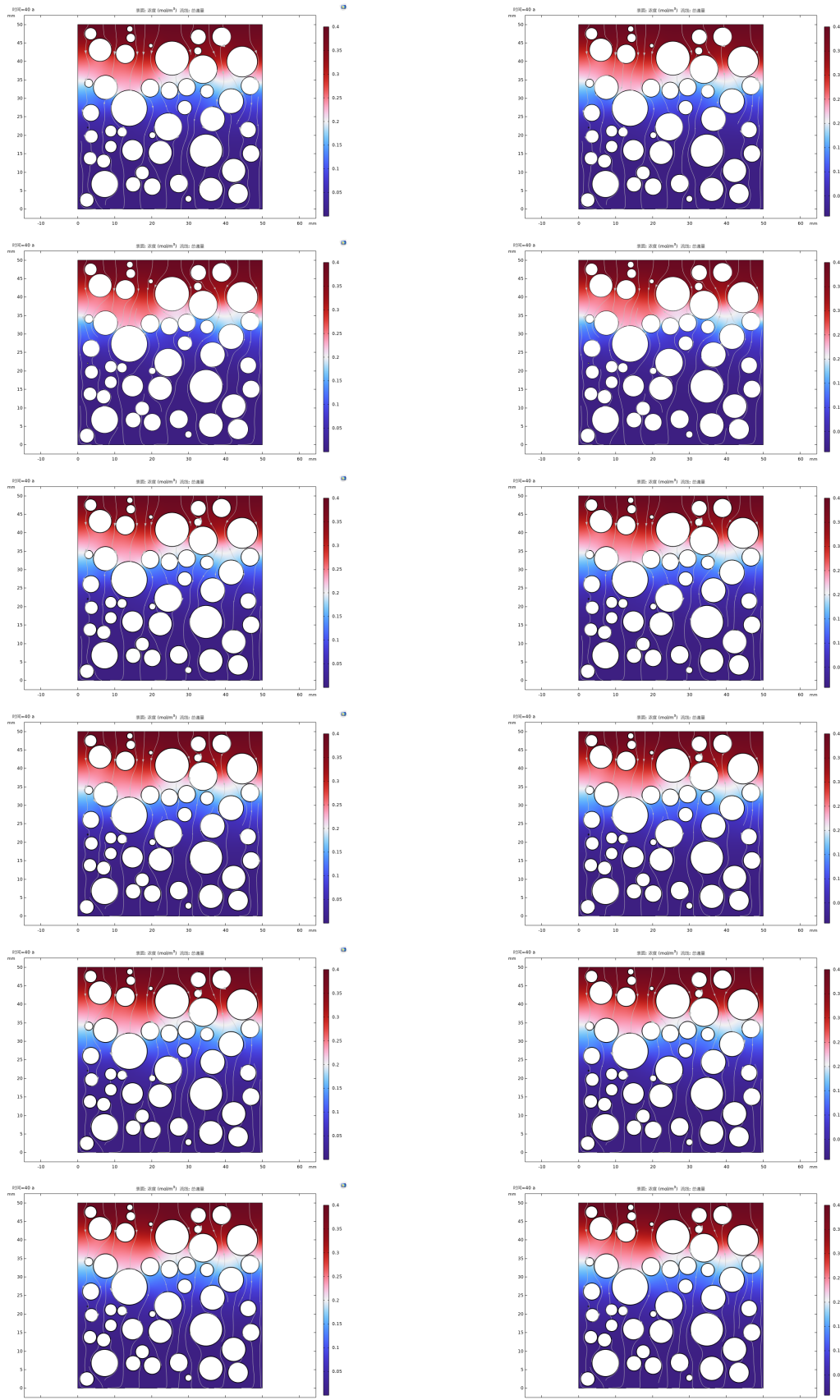
D is the diffusion coefficient of chloride ion, m^2/s ; t is the erosion time, s; C is a chloride ion concentration, %; x is the depth from the concrete surface, m.

2.2 REQUIREMENT OF PROJECT

At 50 mm \times 50 mm concrete member, the surface concentration of chloride ion is 0.5%, the minimum particle size of aggregate is 2.5 mm, the maximum particle size is 10 mm, the aggregate rate is 40 %, and the penetration is 30 years.

From the mesoscale, concrete can be regarded as a three-phase heterogeneous composite material composed of mortar, coarse aggregate, and an interfacial transition zone. In this simulation, the variable is the thickness of the interface thickness region.

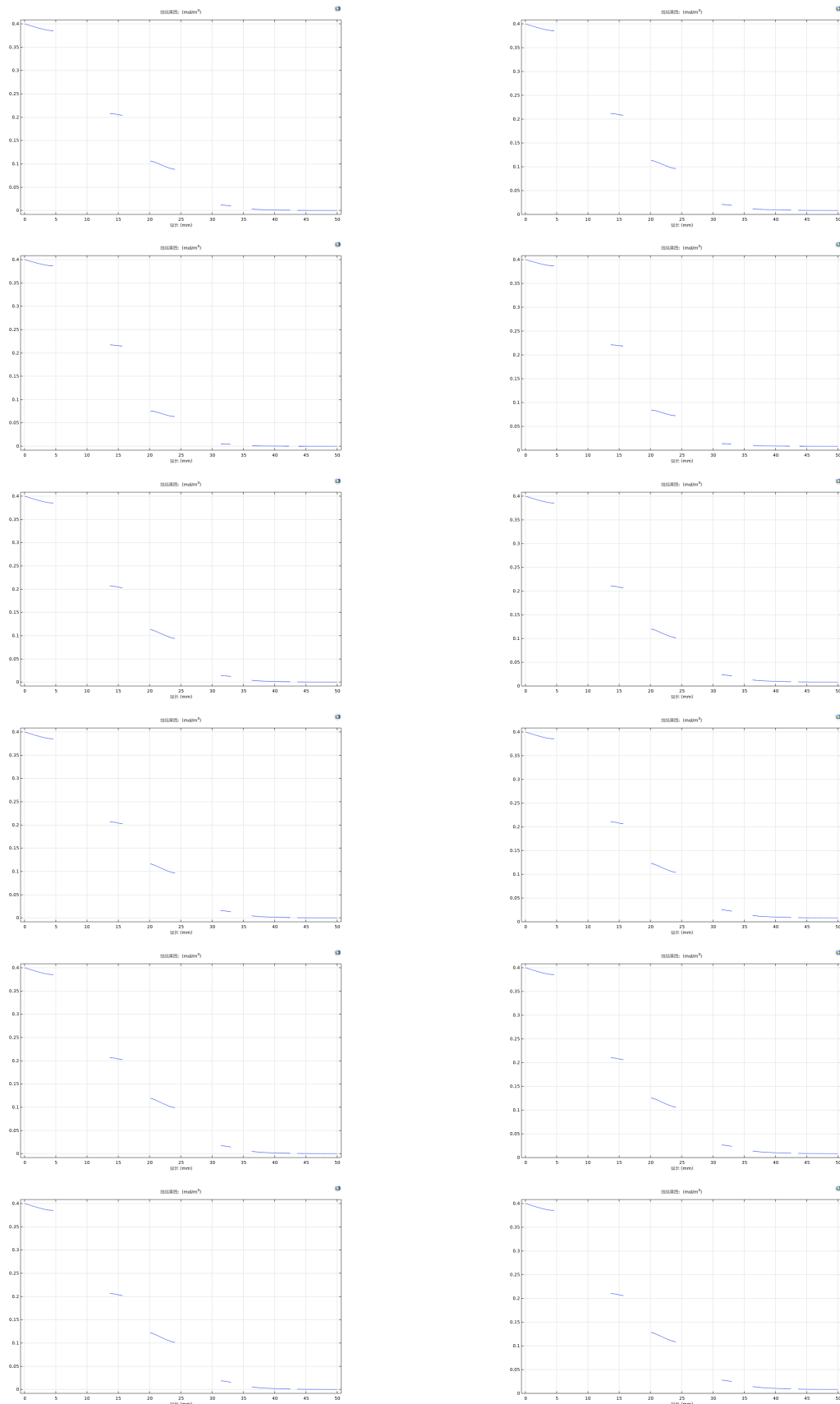




(a) Initial chloride ion concentration in concrete = 0 % (b) Initial chloride ion concentration in concrete = 80 %

FIGURE 3: WHEN THE INITIAL CHLORIDE ION CONCENTRATION INSIDE THE CONCRETE FILLED WITH THE AGGREGATE OF DIFFERENT INTERFACIAL TRANSITION ZONE THICKNESS IS 0 OR 0.008%, THE CONCENTRATION DISTRIBUTION OF CHLORIDE ION PENETRATION FOR 30 YEARS.





(a) Initial chloride ion concentration in concrete = 0 % (b) Initial chloride ion concentration in concrete = 80 %

FIGURE 4: CHLORIDE ION CONCENTRATION DISTRIBUTION CURVE AT THE CENTER LINE OF CONCRETE FILLED WITH THE AGGREGATE OF DIFFERENT INTERFACIAL TRANSITION ZONE THICKNESS.

2.3 SIMULATED RESULT

By using MATLAB to generate aggregate randomly (see the code in the attachment), the aggregate of 1003.9 mm^2 is actually generated, and the actual delivery rate is 40.156 %.

By making the randomly generated aggregate radius satisfy the normal distribution, the aggregate radius is made to satisfy the normal distribution.

In a fixed number of years, the farther away from the surface of the mortar, the lower the chloride ion concentration. This is because chloride ions invade the concrete mainly from the external environment, and the diffusion speed and distance of chloride ions decrease with increasing depth.

The trend of the results of each line is roughly the same, but if the initial concentration of chloride ion is high, the concentration of chloride ion on the corresponding section line is also high. When the initial concentration of chloride ion is 0, the concentration on the corresponding transversal line of different interfaces thickens, and when the initial concentration is 0.008, the concentration increases.

2.4 APPENDIX

```

1 % 50mm*50mm Minimum particle size 2.5mm Maximum particle size 10mm Rate of aggregate placement 40% Penetrate for 30 years
2 % Thickness of interfacial transition zone 60um
3 clc;
4 clear;
5 Rmax=10; % Maximum particle size mm
6 Ragg=0.4; % Aggregate rate
7 a = 50;% mm
8 b = 50;% mm
9 Aagg = Ragg*a*b;% Maximum aggregate area 1000
10 Acum = 0;% Existing aggregate area
11 cum = 0;% Number of circles
12 locate = zeros(1,3);
13
14 % The first time
15 for n = 1:100
16     x = rand(1)*50;% Define aggregate X center coordinates 0~50 mm
17     y = rand(1)*50;% Define aggregate Y center coordinates 0~50 mm
18     % Dm = GenRanNum1(1);% Define a random value for aggregate diameter
19     Dm = 2.5 + 7.5*rand(1);
20     r = Dm/2;
21     if (x + 1.3*r <= 50) && (x - 1.3*r >= 0) && (y + 1.3*r <= 50) && (y - 1.3*r >= 0)% Wall effect
22         Acum = Acum + pi*r^2;% Area accumulation
23         locate = [x y r];% Record position
24         break
25     end
26 end
27
28 while (Acum <= 1000)
29     x = rand(1) * 50;% Define aggregate X center coordinates 0~50 mm
30     y = rand(1) * 50;% Define aggregate Y center coordinates 0~50 mm
31     % Dm = GenRanNum1(1);% Define a random value for aggregate diameter
32     % Dm = 2.5 + 7.5*rand(1);
33     mu = 6.25;          % The mean of a normal distribution
34     sigma = 1.875;       % The standard deviation of the normal distribution
35     Dm = normrnd(mu,sigma); % Generate a random number
36     r = Dm / 2;
37
38     s = size(locate);
39     num = 0;% Reset each time
40
41     if (x + 1.3*r <= 50) && (x - 1.3*r >= 0) && (y + 1.3*r <= 50) && (y - 1.3*r >= 0)% Wall effect
42         for j = 1:s(1) % The coordinates we already have
43             if (circlesOverlap(x, y, r, locate(j,1), locate(j,2), locate(j,3))) % Unsatisfied spacing
44                 num = 1;

```



```

45         break % Any dissatisfaction stops the test
46     end
47 end
48
49 if num == 0 % Satisfy all the time
50     Acum = Acum + pi*r^2;% Area accumulation
51     locate = [locate;x,y,r];% Record position
52 else
53     continue
54 end
55 else
56     continue
57 end
58 end
59
60 hold on
61 theta=0:pi/40:2*pi;% Define the number of points to draw a circle
62 for k = 1:s(1)
63     xx = locate(k,1) + locate(k,3)*cos(theta);
64     yy = locate(k,2) + locate(k,3)*sin(theta);
65     plot(xx,yy, '-')
66 end
67 axis equal;
68 axis([0,50,0,50]);
69
70 function overlap = circlesOverlap(x1, y1, r1, x2, y2, r2)
71 % Determine if two circles overlap.
72 dx = x2 - x1;
73 dy = y2 - y1;
74 d = sqrt(dx^2 + dy^2);
75 if d < 1.05*(r1 + r2)
76     overlap = true;
77 else
78     overlap = false;
79 end
80 end

```



3 FINITE ELEMENT SIMULATION OF OFFSHORE WIND TURBINE BASED ON FLUID-STRUCTURE COUPLING

3.1 BACKGROUND

The superstructure weight has a certain influence on the service mechanical properties of wind power towers in the aspects of structural stability, structural stiffness, dynamic characteristics, and load distribution:

1. *Structural stability*: The heavier superstructure can increase the anti-overturning and anti-lateral load capability of the wind power tower and reduce the tilt risk of the tower.
2. *Structural stiffness*: The heavier superstructure can increase the rigidity of the tower, reduce the structural vibration and deformation, and thus improve the dynamic response and wind resistance of the tower.
3. *Dynamic characteristics*: The weight of the superstructure will affect the natural frequency and modal form of the wind power tower. Heavier superstructures result in lower natural frequencies, which can cause resonance problems and increase the risk of fatigue damage and vibration problems to the structure.
4. *Load distribution*: Heavier superstructures may result in uneven load distribution, increasing stress on some of the connecting and supporting elements, potentially leading to the risk of fatigue failure and structural damage.

3.2 SIMULATION PREPARATION

The tower barrel is in three sections, the upper section is 12.582m in length, 6.5m in diameter, and 24mm in wall thickness; the middle section is a transition section, 162m in length; the lower section is 45m in length, 10m in diameter and 55mm in wall thickness.

Components	Material	Density (kg/m^3)	Young's Modulus (Pa)	Poisson's Ratio
Crane	Structural steel	360	2.06E11	0.28
Columns	Structural steel	7850	2.06E11	0.28
Blades	E-glass	66.18	2.8E10	0.3

TABLE 1: MATERIAL PROPERTIES OF EACH COMPONENT

The part of the tower barrel uses sweeping, namely a hexagonal grid. The edge surface of each segment of the tower barrel uses face meshing, the bottom end is set as a fixed support, and the tower body is selected as a fluid-structure coupling interface.



3.3 SIMULATED RESULT

	60 (m)	80 (m)	100 (m)	120 (m)
Total Deformation	1.096E-03	1.175E-03	1.253E-03	1.328E-03
Directional Deformation	8.647E-04	9.344E-04	9.344E-04	9.344E-04
Equivalent Elastic Strain	1.253E-05	1.341E-05	1.341E-05	1.341E-05
Maximum Principal Elastic Strain	1.367E-05	1.463E-05	1.463E-05	1.463E-05
Maximum Shear Elastic Strain	1.776E-05	1.900E-05	1.900E-05	1.900E-05
Equivalent Stress	2.582E+06	2.762E+06	2.762E+06	2.762E+06
Maximum Principal Stress	3.204E+06	3.429E+06	3.429E+06	3.429E+06
Maximum Shear Stress	1.429E+06	1.529E+06	1.529E+06	1.529E+06
Strain Energy	6.926E-02	7.909E-02	7.909E-02	7.909E-02

TABLE 2: MECHANICAL PROPERTIES OF DIFFERENT TURBINE BLADE DIAMETERS

Through the data obtained from the simulation results, it is found that except for the total deformation, other mechanical properties values of the three groups are the same for 80m, 100m, and 120m, which may be caused by the step size setting of only 100. If the step size is increased, the differences between them will appear.

For the total deformation, as shown in Figure 5, the larger the diameter of the fan blade is, that is, the larger the upper load is, the larger the shape variable of the tower barrel is, but their order of magnitude is in the class of millimeters.

By comparing the data of the 60m group and the 80m group in Table 2, it can be seen that with the increase in blade diameter, the values of total deformation, x-direction deformation, principal elastic strain, shear elastic strain, principal stress, shear stress, strain energy, and other parameters increase.

3.4 DIFFICULTIES ENCOUNTERED IN THE SIMULATION

- The computer equipment itself is unable to connect the coupling system;
- For various properties of materials, the unit is not carefully identified, resulting in a lot of wasted time and energy;
- The step length is set short, only 100 steps, which does not make the difference in the calculation example with a larger fan blade diameter.



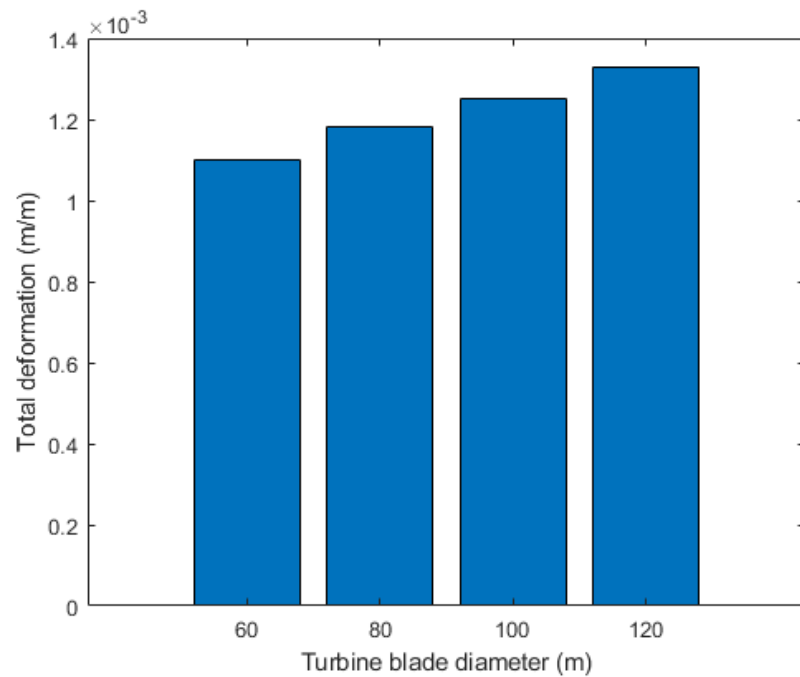


FIGURE 5: TOTAL DEFORMATION OF DIFFERENT SUPERSTRUCTURE WEIGHTS

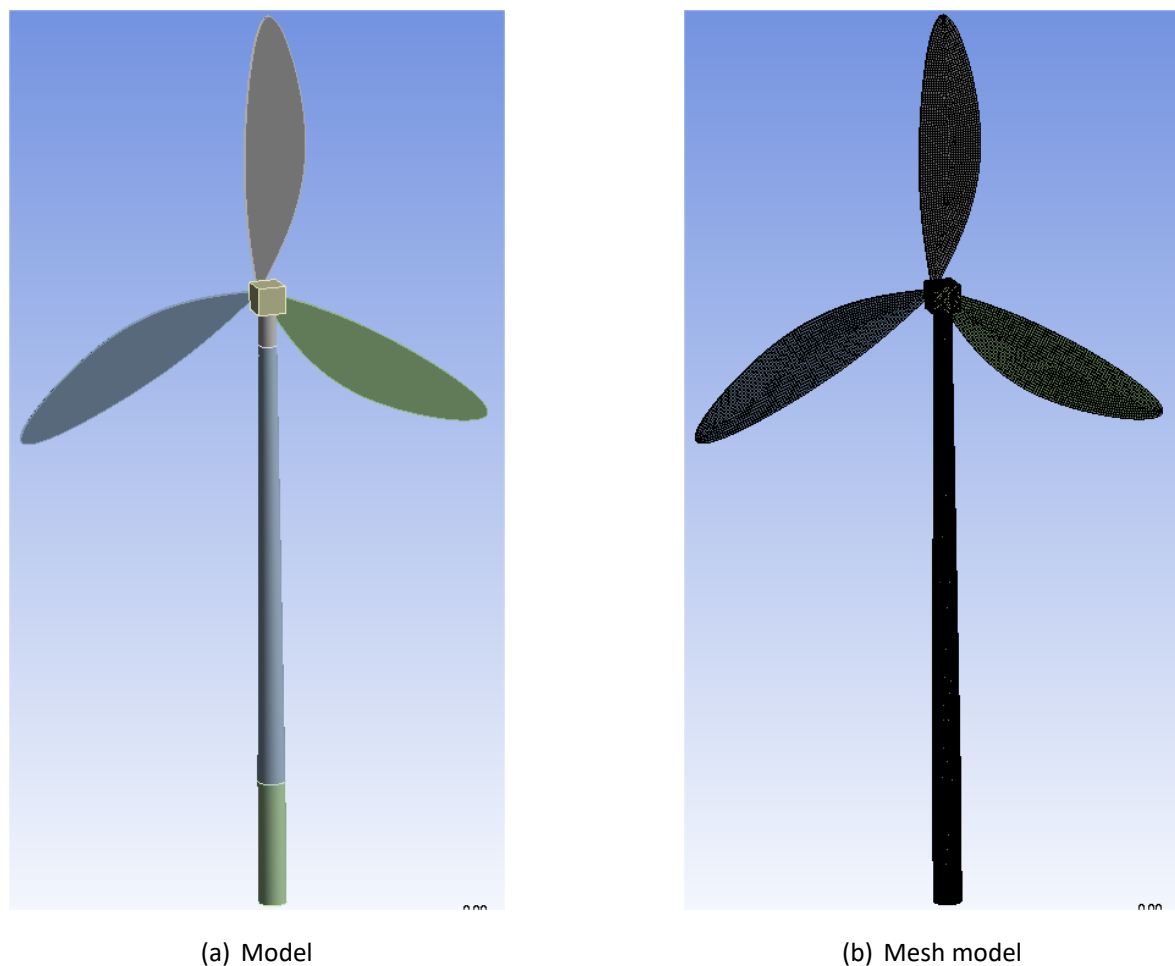


FIGURE 6: WIND TURBINE MODEL

4 FINITE ELEMENT SIMULATION AND FAILURE STUDY OF LATERAL WELL

4.1 BACKGROUND

Multilateral wells — those with multiple legs that branch off from a single conduit — can produce oil efficiently because the legs can tap multiple productive zones and navigate around impermeable ones. Unfortunately, drilling engineers must often mechanically stabilize multilateral wells with a liner or casing, which can cost millions of dollars. Leaving the wellbore uncased reduces construction costs, but it runs a relatively high risk of catastrophic failure both during installation and after pumping begins.

The poroelastic simulations estimate 3D compaction related to pumping by taking subsurface fluid flow with Darcy's law and coupling it to structural displacements with a stress-strain analysis. This project focuses on elastic displacements brought on by changing fluid pressures when pumping begins. Related analyses for elastoplastic deformations are straightforward using material laws automated in the Structural Mechanics Module, Nonlinear Structural Materials Module, and Geomechanics Module.

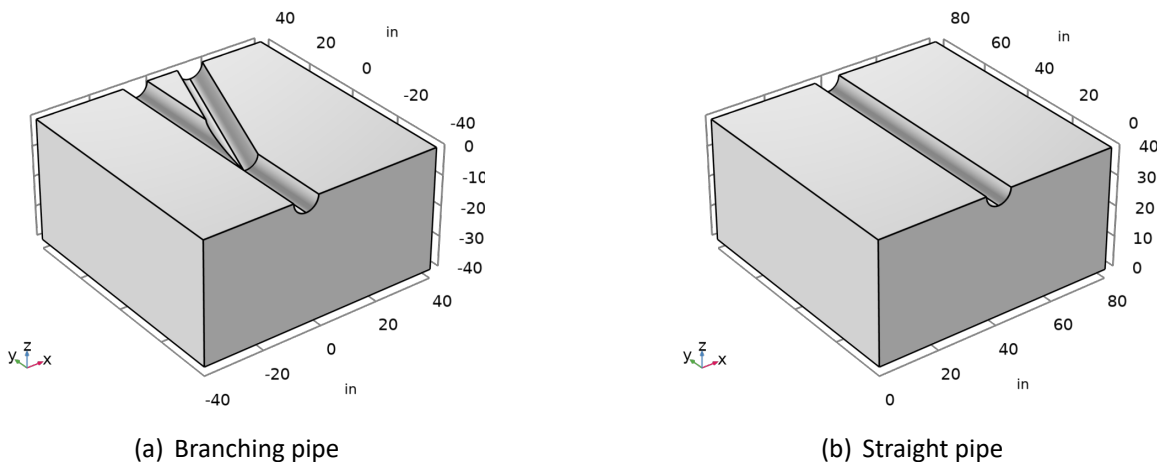


FIGURE 7: GEOMETRY FOR AN ANALYSIS OF A HORIZONTAL OPEN-HOLE MULTILATERAL WELL AND A VERTICAL WELL.

4.2 SIMULATION PREPARATION

The modeled geometry (Figure 1) is the lower half of a branching junction, a segment from a larger well network. The junction lies roughly 25 feet from the start of the well. The entire well network extends much further, perhaps hundreds of feet. The well is 8.5 inches in diameter and sits in a cube of 80 inches on each side. Pumps move fluid from the reservoir into the well. Fluid exits the geometry only through the well. The displacement at the reservoir edge is constrained. The walls of



the well, however, deform freely. The goal is to solve for the change in fluid pressure, stress, strain, and displacement that the pumping causes rather than their absolute values.

4.2.1 FLUID FLOW

To describe fluid flow, you insert the Darcy velocity into an equation of continuity

$$\nabla \cdot \left[-\frac{\kappa}{\mu} \nabla p \right] = 0$$

where κ is the permeability, μ is the dynamic viscosity, and p equals the pressure of the oil in the pores.

For the flow boundaries, you already know the change in fluid pressure from the well to the reservoir edge. The planar surface adjacent to the well (between the upper and lower blocks) is a symmetry boundary. Because the well is the only exit for the fluid, there is no flow to or from connecting well segments.

4.2.2 SOLID DEFORMATION

The system of equations that describes the quasi-static deformation is

$$-\nabla \cdot \sigma = F$$

where σ denotes the stress tensor, and F are external body forces. The stress tensor is augmented by the pressure load due to changes in pore pressure. In this model, the Biot-Willis coefficient is equal to one.

4.2.3 FAILURE CRITERION

The 3D Coulomb failure criterion relates rock failure, the three principal stresses (σ_1 , σ_2 , and σ_3), and the fluid pressures as follows:

$$fail = (\sigma_3 + p) - Q(\sigma_1 + p) + N(1 + \frac{(\sigma_2 - \sigma_1)}{(\sigma_3 - \sigma_1)}), Q = \frac{1 + \sin\phi}{1 - \sin\phi}, N = \frac{2\cos\phi}{1 - \sin\phi} So$$

Here So is the Coulomb cohesion and ϕ is the Coulomb friction angle. When properly calibrated, $fail = 0$ indicates the onset of rock failure; $fail < 0$ denotes catastrophic failure, and $fail > 0$ predicts stability. Because this model solves for the pressure change brought on by pumping as well as the stresses, strains, and displacements that the pressure change triggers, it calculates the expression just given using the change in pressure than its absolute value.

4.3 SIMULATED RESULT

This project couples fluid flow and solid deformation for a poroelastic analysis. The analysis provides estimates of the pressure change brought on by pumping as well as the stresses, strains, and



VARIABLE	DESCRIPTION	VALUE
ρ_f	Fluid density	$0.0361 lb/in^3$
κ	Permeability	$1 \cdot 10^{-13} in^2$
μ	Fluid dynamic viscosity	$1 \cdot 10^{-7} psi \cdot s$
E	Young's modulus	$0.43 \cdot 10^6 psi$
ν	Poisson's ratio	0.16
ρ_s	Solids density	$0.0861 lb/in^3$
ρ_r	Pressure in reservoir	122.45 psi
ρ_w	Pressure in well	0 psi

TABLE 3: MODEL PARAMETER.

VARIABLE	DESCRIPTION	VALUE1	VALUE2
ρ_s	Solids density	$0.0939 lb/in^3$	$0.0861 lb/in^3$
ν	Poisson's ratio	0.4	0.16

TABLE 4: MODEL PARAMETER VARIABLE.

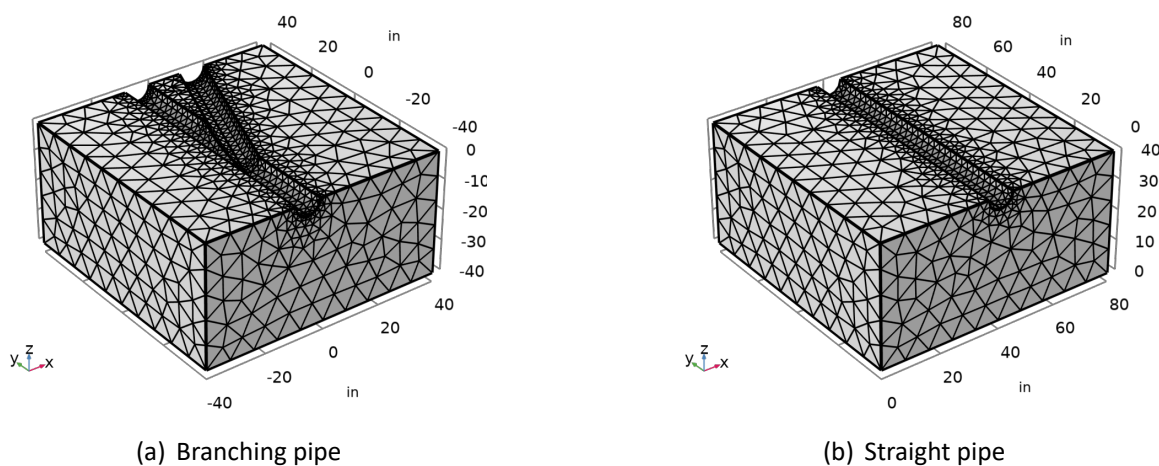


FIGURE 8: MESH FOR AN ANALYSIS OF A HORIZONTAL OPEN-HOLE MULTILATERAL WELL AND A VERTICAL WELL.

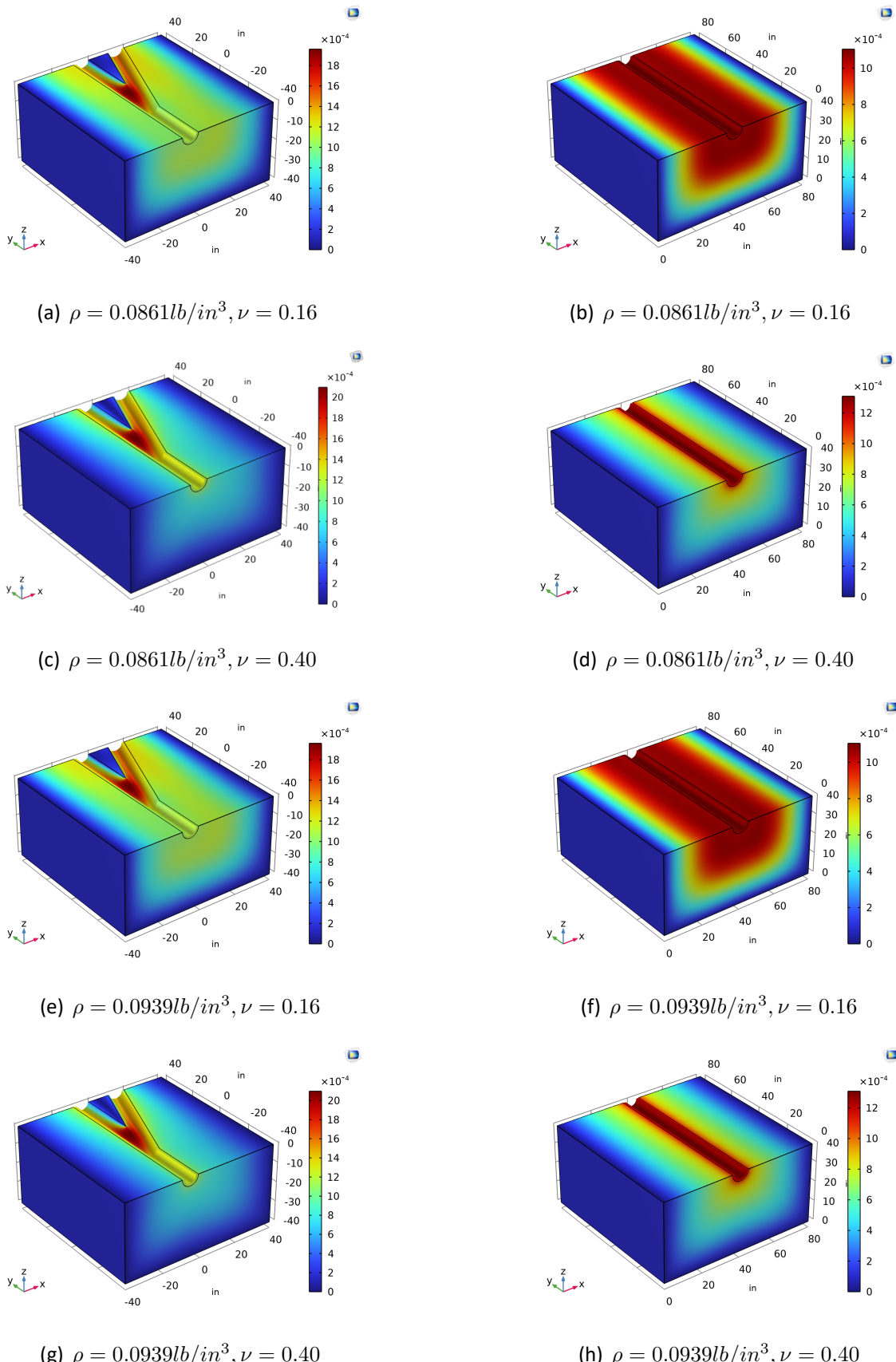


FIGURE 9: COMSOL MULTIPHYSICS ESTIMATES OF DISPLACEMENT. SHADING INDICATES THE TOTAL DISPLACEMENT AND THE GEOMETRY APPEARS AS LINES. EVEN AS THE DEFORMED SHAPESHIFTS, THOSE LINES REMAIN STEADY; THE SHADED IMAGE SHOWS MOVEMENT RELATIVE TO THE GEOMETRY OUTLINES.



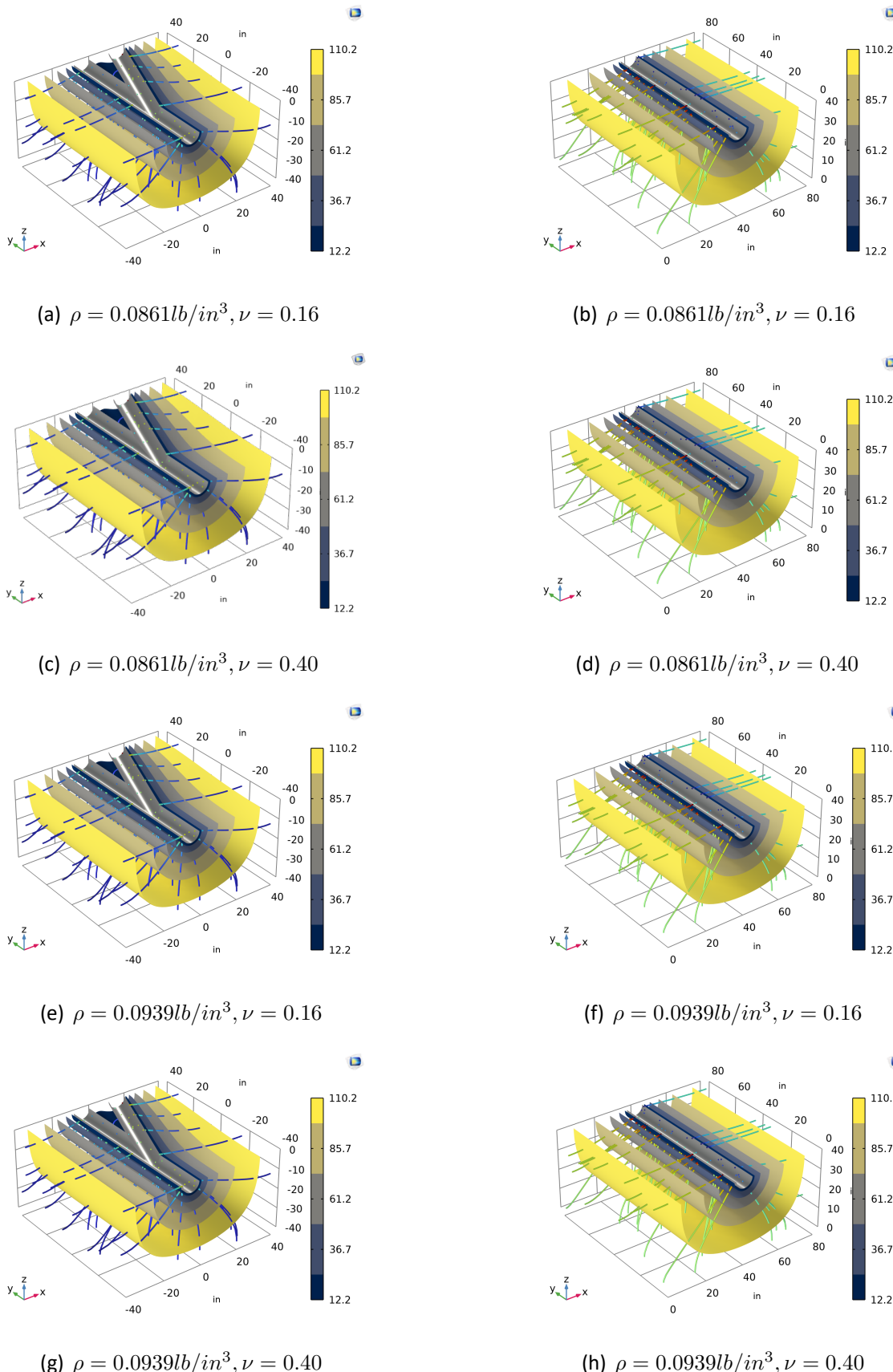


FIGURE 10: COMSOL MULTIPHYSICS POREOELASTIC ANALYSIS OF A MULTILATERAL AND A STRAIGHT WELL. THE RESULTS ARE FLUID PRESSURE (THE ISOSURFACES), PRESSURE GRADIENT (STREAMLINES), AND FLUID VELOCITIES (STREAMLINE SHADING).



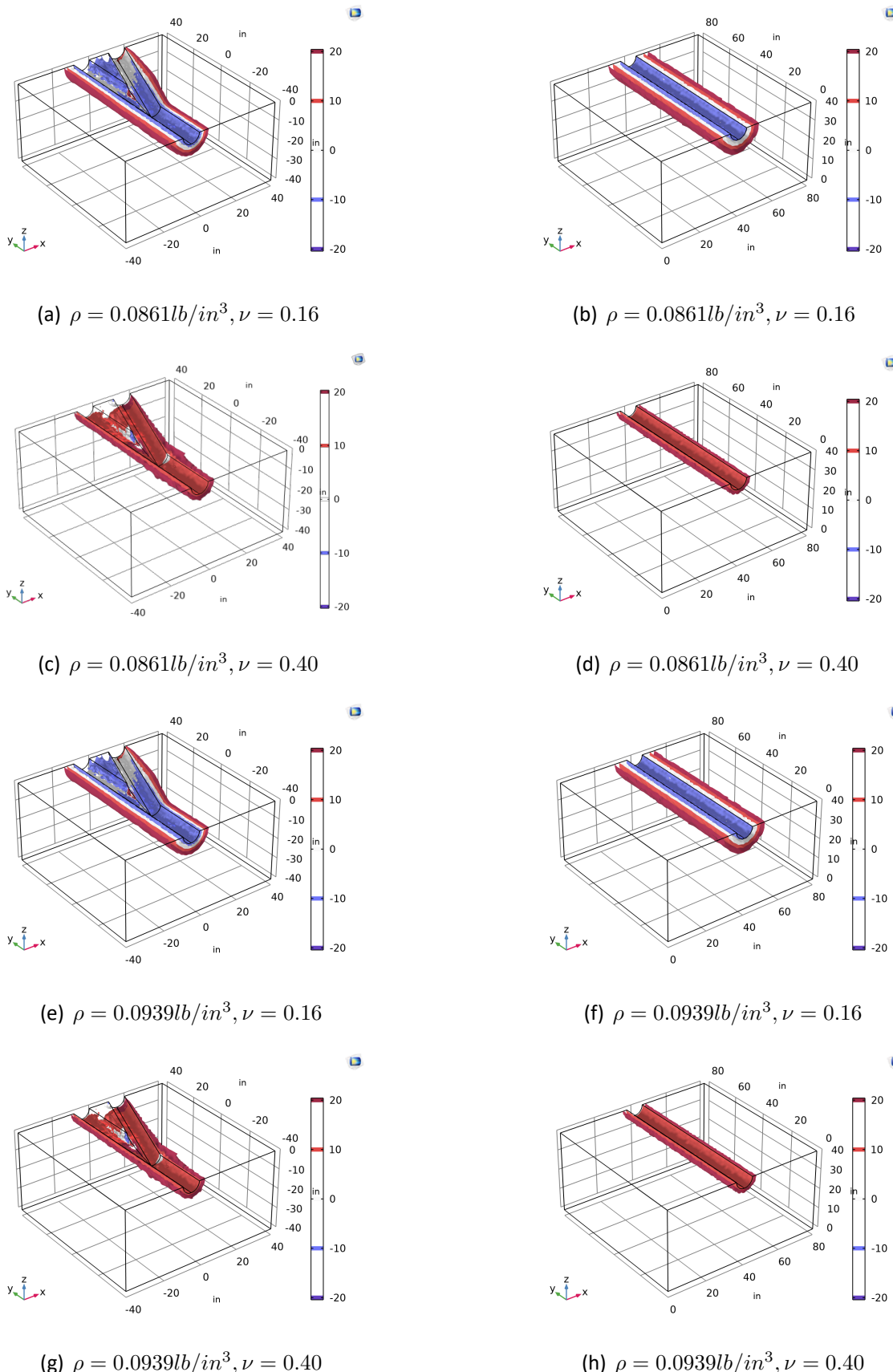


FIGURE 11: VALUES OF THE FAIL FUNCTION CALCULATED WITH RESULTS FROM A POREOELASTIC MODEL FOR THE BRANCHING JUNCTION IN AN OPEN-HOLE MULTILATERAL WELL. A NEGATIVE VALUE FOR THE FAIL FUNCTION DENOTES A GREATER POTENTIAL FOR FAILURE.



displacements that the pressure drop triggers. Combining the simulation results with a 3D Coulomb failure expression maps vulnerability to mechanical failure from the pumping.

Branch section analysis: The most likely failure place of the four models is in the middle area of the two-branch pipeline; The maximum strain value of the model is located right above the fracture in the well, and with the change of solid density and Poisson's ratio, the maximum strain variable does not change obviously, and the influence range of deformation does not change much. The trend of pressure lipolytic surface and streamline is roughly the same.

Analysis of the main section: the maximum strain value of the model is located right above the main section, and with the change of solid density and Poisson's ratio, the maximum strain variable increases with the increase of Poisson's ratio, and the influence range of deformation has little change. When Poisson's ratio is 0.16, the place with the greatest possibility of failure is right above the main section. When Poisson's ratio is 0.4, the possibility of failure of the model is very low. The trend of pressure lipolytic surface and streamline is roughly the same.



5 ACKNOWLEDGMENTS

I am deeply indebted to Prof. Wei for his guidance in the lecture classes; Senior M.Y. Liang, for his soul of patience and working with us to solve the problems that inevitably arise. This report is dedicated to OCE326 for the fall 2023 semester, a nice experience.

